Spiroiminodihydantoin Lesions Derived from Guanine Oxidation: Structures, Energetics, and Functional Implications[†]

Lei Jia,[‡] Vladimir Shafirovich,[‡] Robert Shapiro,[‡] Nicholas E. Geacintov,[‡] and Suse Broyde*[,‡,§]

Department of Chemistry, New York University, New York, New York 10003, and Department of Biology, New York University, New York, New York 10003

Received December 15, 2004; Revised Manuscript Received February 18, 2005

ABSTRACT: Reactive oxygen species present in the cell generate DNA damage. One of the major oxidation products of guanine in DNA, 8-oxo-7,8-dihydroguanine, formed by loss of two electrons, is among the most extensively studied base lesions. The further removal of two electrons from this product can yield spiroiminodihydantoin (Sp) *R* and *S* stereoisomers. Both in vitro and in vivo experiments have shown that the Sp stereoisomers are highly mutagenic, causing G → T and G → C transversions. Hence, they are of interest as examples of endogenous DNA damage that may initiate cancer. To interpret the mutagenic properties of the Sp lesions, an understanding of their structural properties is needed. To elucidate these structural effects, we have carried out computational investigations at the level of the Sp-modified base and nucleoside. At the base level, quantum mechanical geometry optimization studies have revealed exact mirror image symmetry of the *R* and *S* stereoisomers, with a near-perpendicular geometry of the two rings. At the nucleoside level, an extensive survey of the potential energy surface by molecular mechanics calculations using AMBER has provided three-dimensional potential energy maps. These maps reveal that the range and flexibility of the glycosidic torsion angles are significantly more restricted in both stereoisomeric adducts than in unmodified 2′-deoxyguanosine. The structural and energetic results suggest that the unusual geometric, steric, and hydrogen bonding properties of these lesions underlie their mutagenicity. In addition, stereoisomer-specific differences indicate the possibility that their processing by cellular replication and repair enzymes may be differentially affected by their absolute configuration.

Reactive oxygen species (ROS)[1] present in the cell, or produced by ionizing radiation, can generate a variety of DNA damage (*1*−*4*), including strand breaks, protein−DNA cross-links, abasic sites, and base lesions (*2*, *3*, *5*−*8*). If the damage is not removed by repair enzymes, the processing of the damaged DNA by polymerases may cause mutations and, ultimately, cancer. Colorectal, lung, kidney, head and neck, and breast cancers in humans have been linked to tumor initiation by ROS (*9*−*15*). In addition, reactive oxygen species have been associated with aging, and studies with rodents suggest that aging is indeed related to oxidative DNA damage (*16*−*19*).

One of the major oxidation products of guanine in DNA, produced through a loss of two electrons, is 8-oxo-7,8-dihydroguanine (8-oxoG) (*20*). Since 8-oxoG has a lower redox potential than guanine, it can easily be further oxidized (*21*−*23*) to produce cyanuric acid (Ca), oxaluric acid (Oa), and oxazolone (Oz) (*24*). Other oxidation products of guanine, namely, imidazolone (Iz) and nitroimidazole (NI), have also been prepared (*25*). These are all highly mutagenic. In vivo studies in *Escherichia coli* have shown that Ca, Oz, and Oa are readily bypassed and efficiently cause G → T transversion mutations (*26*). Iz is bypassed somewhat less efficiently, but readily produces G → C transversion mutations when it is not blocking. NI and urea (Ua) (which is derived from Oa) are more blocking, but are also mutagenic. NI permits incorporation of all four nucleotides opposite the lesion, while Ua, when bypassed, causes almost exclusively G → T transversions (*27*, *28*).

Recent studies have also shown that the further removal of two electrons from 8-oxoG can produce spiroiminodihydantoin (Sp) diastereoisomers, guanidinohydantoin (Gh), and its rearrangement isomer iminoallantoin (Ia); these can also be formed directly from guanine by a variety of oxidizing agents (*29*−*39*). We focus on the Sp diastereoisomers in this paper. The *R* and *S* stereoisomers of Sp are depicted in Figure 1.

Biological processing of the Sp lesions has been of considerable recent interest because of the possibility that they may occur endogenously and contribute to human cancer (*21*). Our current understanding of how such DNA damage may initiate cancer involves the induction of mutations in oncogenes or tumor suppressors during replication, if the lesion fails to be accurately repaired (*40*, *41*).

[†] This research is supported by NIH Grant CA-75449 to S.B. and NIH Grant ES-11589 to V.S. and N.E.G.

* To whom correspondence should be addressed. Telephone: (212) 998-8231. Fax: (212) 995-4015. E-mail: broyde@nyu.edu.

[‡] Department of Chemistry.

[§] Department of Biology.

[1] Abbreviations: ROS, reactive oxygen species; 8-oxoG, 8-oxo-7,8-dihydroguanine; Ca, cyanuric acid; Oa, oxaluric acid; Oz, oxazolone; Iz, imidazolone; NI, nitroimidazole; Ua, urea; Sp, spiroiminodihydantoin; BER, base excision repair; KF, Klenow fragment; Fpg, formamidopyrimidine glycosylase; MutY, adenine DNA glycosylase; yOGG, yeast 8-oxoG glycosylase; hOGG, human 8-oxoG glycosylase; NEIL, endonuclease VIII-like; dG, 2′-deoxyguanosine; DFT, density functional theory; QM, quantum mechanics; NDB, Nucleic Acid Database.

10.1021/bi0473657 CCC: $30.25
Published on Web 03/31/2005

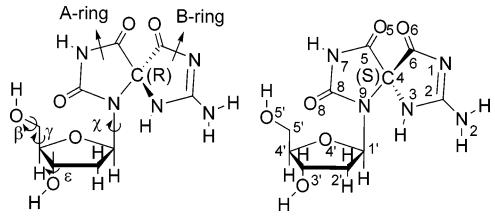

FIGURE 1: Structures of spiroiminodihydantoin *R* and *S* stereoisomer deoxyribonucleosides. At the base level, the sugar is replaced by a hydrogen. Torsion angles are defined for the *R* stereoisomer deoxyribonucleoside. Atom numbers are defined for the *S* stereoisomer deoxyribonucleoside.

Most oxidative DNA damage is repaired by base excision repair (BER) pathways (*42*−*44*). The *E. coli* BER glycosylase Fpg, which removes 8-oxoG and a variety of other oxidized purine lesions, removes both of the Sp stereoisomers efficiently when paired with any of the four different DNA bases in the complementary strand. The *E. coli* adenine glycosylase MutY, which can remove adenine mispaired with 8-oxoG, is unable to remove adenine when paired with Sp (*45*). The functionally related yeast enzymes yOGG1 and yOGG2 also remove Sp when paired with any of the four natural DNA bases in a duplex, while the human homologue hOGG1 cannot remove Sp in any base pairing context (*46*). However, the mammalian BER glycosylase NEIL1 is able to excise these lesions opposite the four natural bases in double-stranded DNA (*47*).

The processing of the Sps by several DNA polymerases has also been investigated. In vitro primer extension studies with pol α and pol *β* show that the Sp lesions block extension beyond the lesion (*48*). However, guanine or adenine is inserted opposite the Sp lesions by KF exo$^-$ even more efficiently than opposite 8-oxoG, although subsequent extension is significantly blocked. The insertion of adenine is favored over guanine, while incorporation of cytosine opposite Sp is not observed (*49*). In vivo studies of DNA containing site-specifically modified Sp transfected into *E. coli* show that DNA polymerases are largely blocked by both Sp stereoisomers, but that G → C and G → T transversion mutations result upon bypass of the lesions. It was found that the two Sp stereoisomers were both more blocking and more mutagenic than 8-oxoG (*50*). The Sps are more blocking than Ca, Iz, Oz, Gh, and Oa, but when bypassed, they are highly mutagenic (*28*, *50*).

To interpret the mutagenic potentials of the Sp stereoisomeric lesions and their response to DNA repair enzymes, an understanding of their structural properties is needed. However, such structural information is at present not available. To elucidate the structural and conformational properties of these novel lesions, we have carried out computational investigations at the level of the modified base and Sp nucleoside. At the base level, quantum mechanical geometry optimization studies reveal the exact mirror image symmetry of the *R* and *S* stereoisomers, with a near-perpendicular geometry of the two rings. At the nucleoside level, an extensive survey of the potential energy surface by molecular mechanics calculations using AMBER provides three-dimensional potential energy maps. These maps reveal that the range and flexibility of glycosidic torsion angles are significantly more restricted in both Sp stereoisomers than in unmodified 2′-deoxyguanosine (dG). Our results indicate that the novel geometric, steric, and hydrogen bonding properties of these lesions underlie their mutagenicity. Moreover, stereoisomer-specific differences suggest the possibility that processing of these lesions by cellular replication and repair enzymes may be affected by their differing absolute configurations.

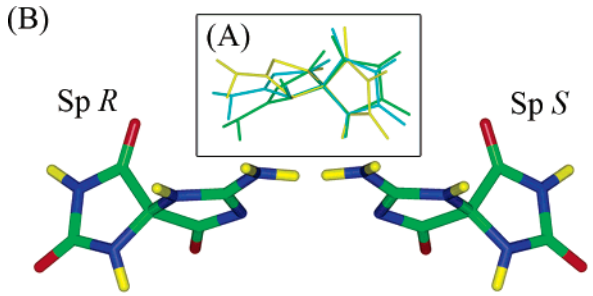

FIGURE 2: (A) Overlay of the combination of nine starting structures for quantum mechanical geometry optimization. (B) Structures of Sp *R* and *S* stereoisomers after geometry optimization.

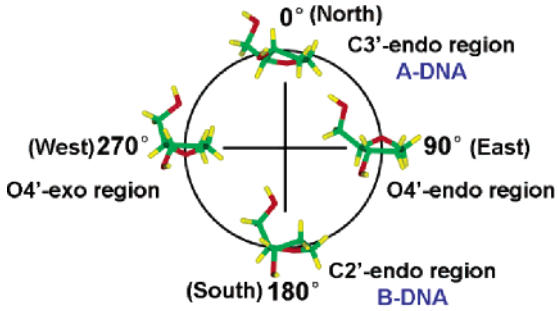

FIGURE 3: Deoxyribose pseudorotation cycle showing sugar conformations as a function of pseudorotation parameter *P*. The five-membered sugar rings are nonplanar, with one or two atoms out of plane. The sugar puckering pseudorotation angle treats the nonplanarity as a wave going around the ring (*56*).

METHODS

Quantum Mechanical Geometry Optimization of Sp on the Base Level. Nine different starting models of the Sp *R* and *S* stereoisomers were built with SPARTAN from Wavefunction, Inc. They were modeled to consider all possibilities for puckering of the sp^3 hybridized C4 atom connecting the two rings (Figures 1 and 2A); preliminary geometry-optimized structures were obtained using constraints to preserve the initial ring dihedral angles (Table S1) with the MERCK molecular force field (MMFF94) (*51*) in SPARTAN. In the next stage, we used the quantum mechanical density functional theory (DFT) method (B3LYP/6-31G*) (*52*, *53*) in Gaussian 98 (*54*) from Gaussian, Inc., to perform high-level geometry optimizations. The structure of a standard guanine was taken from the NDB (*55*). Identical protocols were employed for amino and imino tautomers of Sp.

Molecular Mechanics Calculations for Sp Deoxynucleosides and Unmodified dG. A library which contained deoxyribose sugar conformations, varying in the sugar pucker pseudorotation parameter *P* (*56*, *57*) from 0° to 355° at 5° intervals, was computed with DUPLEX (*58*) to produce 72 different sugar conformations, spanning the full geometric range for the sugar conformation (Figure 3). The QM geometry-optimized Sp *R* and *S* stereoisomers and unmodified guanine were linked to each of these sugar conformations. Torsion angles *β* (C4′−C5′−O5′−H5′) and *ϵ* (C4′−

C3′−O3′−H3′) were set to 180°. Glycosidic torsion angle χ (C4−N9−C1′−O4′) and the C4′−C5′ linkage γ (C3′−C4′−C5′−O5′) were also surveyed at 5° intervals. In combination, we therefore have $(360/5)^3 = 72^3 = 373\,248$ different conformations for Sp *R* and *S* stereoisomer deoxynucleosides and unmodified dG, which provides a good survey of the whole potential energy surface.

The energy calculations were carried out with AMBER 5.0 (*59*) with the Cornell et al. force field (*60*) and PARM99 parameter set (*61*). To parametrize the force field for the Sp stereoisomers, we computed partial charges compatible with the rest of the force field by QM (HF/6-31G*) with Gaussian 98 (*54*). One *syn* ($\chi = 60°$) and one *anti* ($\chi = 240°$) conformation for each modified deoxynucleoside were used for the partial charge calculations. The least-squares charge fitting algorithm Restrained Electrostatic Potential (RESP) (*62*) provided with AMBER 5.0 was used to fit the charge to each atomic center. The final partial charges were determined by averaging partial charges of *syn* and *anti* conformations. Missing bond angle parameters were obtained using equilibrium bond angles from the QM optimized structures with force constants chosen from chemically analogous ones already present in the force field. These added Sp parameters are given in Table S3. All other parameters for the Sp moieties were already present in the PARM99 parameter set. AMBER atom type assignments and partial charges are given in Table S4. A sigmoidal distance-dependent dielectric function (*63*) was used to implicitly treat solvation in the electrostatic term of the force field.

TECPLOT10 from Amtec Engineering, Inc., was employed to generate three-dimensional energy maps. INSIGHT II from Accelrys, Inc., was employed for visualization and model building.

Calculation of Statistical Weight. The fractional statistical weight of each conformer was calculated by the expression (*64*, *65*)

$$P_{i,j,k} = \frac{e^{-\Delta E_{i,j,k}/RT}}{\sum_{i=1}^{72}\sum_{j=1}^{72}\sum_{k=1}^{72} e^{-\Delta E_{i,j,k}/RT}}$$

where $\Delta E_{i,j,k}$ is the relative energy calculated for a given conformer in kilocalories per mole with respect to the lowest-energy structure, *R* is the universal gas constant (1.987×10^{-3} kcal mol^{-1} K^{-1}), *T* is the temperature (300 K), and *i*, *j*, and *k* represent variables χ, γ, and *P*, respectively. The combined statistical weight for each pairwise two-dimensional surface W_i is given by

$$W_i = \sum_{j=1}^{72}\sum_{k=1}^{72} P_{i,j,k}$$

Computations were carried out on our own cluster of Silicon Graphics Octane workstations.

RESULTS

Quantum Mechanical Geometry Optimizations of R and S Sp Stereoisomers on the Base Level Show a Propeller-like Mirror Image Pair. In the first stage of this study, we created nine different conformations for the Sp *R* and *S* stereoisomers based on different puckering possibilities at the tetrahedral C4 atom, as described in Methods (Figures 1 and 2A), and carried out quantum mechanical geometry optimization for each structure using the quantum mechanical DFT method (B3LYP/6-31G*). Our results show that for each stereoisomer the quantum mechanical geometry optimization produces convergence to a single structure. The final *R* and *S* stereoisomer structures are mirror images (Figure 2B), and the two rings of Sp are nearly flat and essentially perpendicular to each other (Figure 4 and Table S1). These results rule out conformational flexibility at the C4 atom in the Sp stereoisomers.

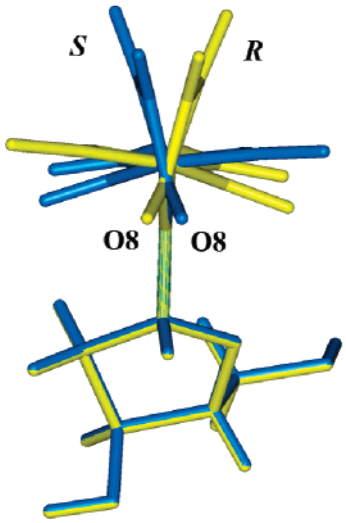

FIGURE 4: Superimposition of Sp *R* and *S* stereoisomer deoxyribonucleosides showing the mirror-image orientation of the pucker in the five-membered rings of Sp. The sugar conformations are the same in both cases ($P = 160°$ and $\gamma = 180°$). The glycosidic torsion χ is 35° for *R* Sp and 70° for *S* Sp.

In these gas phase geometry-optimized structures, the amino groups of Sp are nonplanar, as is usually the case for such computed structures (*66*, *67*). However, in all crystal structures of guanines and adenines, the amino group is planar (*55*, *68*, *69*), and we therefore remodeled them as planar for the next stage of our studies involving the modified nucleosides.

Three-Dimensional Energy Maps of Unmodified dG and Sp R and S Stereoisomeric Deoxynucleosides. Three-dimensional potential energy maps were constructed for the Sp *R* and *S* stereoisomer deoxynucleosides, as well as for unmodified dG for comparison. We surveyed three flexible parameters, glycosidic torsion angle χ, C4′−C5′ torsion γ, and sugar pucker pseudorotation parameter *P* (*56*, *57*) at 5° intervals in combination, for a total of 373 248 conformations for each molecule. Energies were evaluated for each conformation using the AMBER suite of programs. Statistical weights based on these energies were computed as described in Methods.

The three-dimensional energy maps are shown in Figure 5. There are limited allowed regions characteristic of deoxynucleosides, with glycosidic bond orientations in *syn* and *anti* domains, C4′−C5′ torsions in the *gauche*$^+$ (60°), *trans* (180°), and *gauche*$^-$ (300°) regions, and sugar puckers spanning C3′-endo ($P = 0°$, North) through O4′-endo ($P = 90°$, East) to C2′-endo ($P = 180°$, South) (*70*) (Figure 3). The O4′-exo region ($P = 270°$, West) is disfavored due to

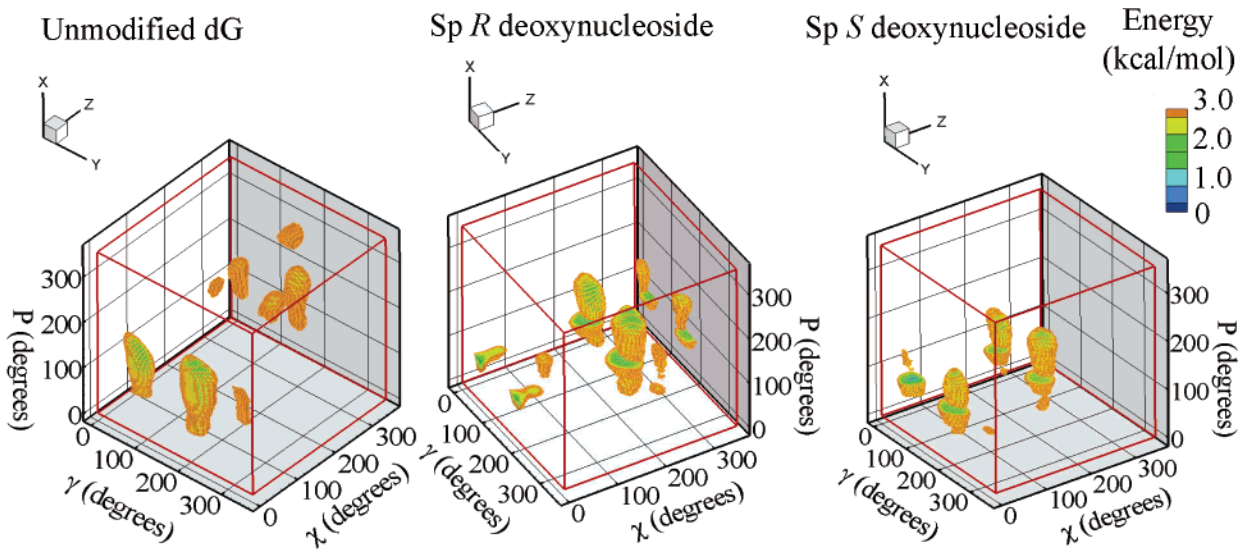

FIGURE 5: Three-dimensional energy maps with relative energies to 3 kcal/mol.

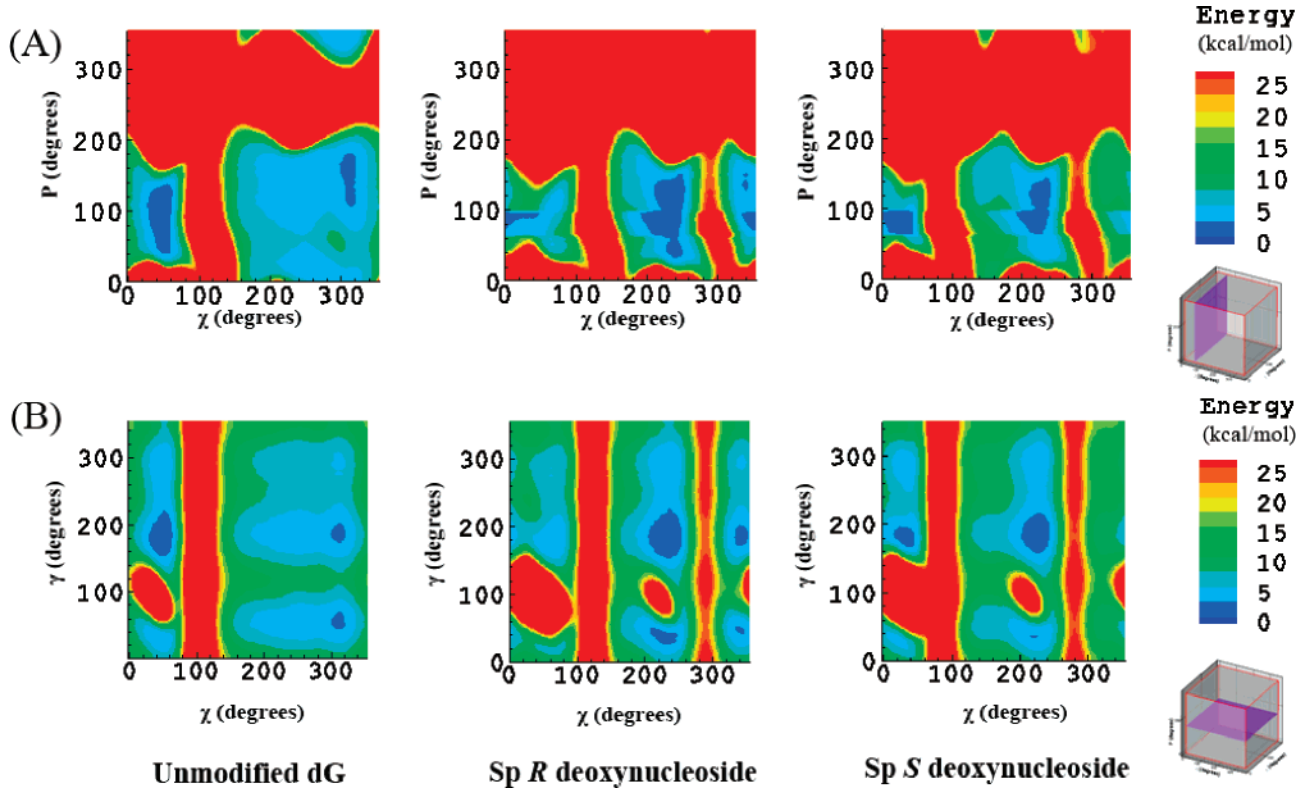

FIGURE 6: Energy map cross sections: (A) $\gamma = 60°$; (B) $P = 160°$, C2′-endo.

a steric conflict between the base and the C5′ exocylic substituents (*57*, *71*, *72*).

Important details of these energy topographies are seen clearly in slices through the three-dimensional surfaces. Figure 6A shows slices through the B-DNA (*73*) $\gamma = 60°$ domain. The important feature of these maps is the identification of two high-energy barriers separating *syn* and *anti* regions in the glycosidic bond rotation for the Sp stereoisomers, but only one such barrier for dG. Figure 6B shows a second plane through the three-dimensional energy surface, through the $P = 160°$ B-DNA C2′-endo sugar pucker. In this cross section, we can more clearly observe the pair of barriers in glycosidic rotation χ for Sp but not the normal dG. We note that these barriers are independent of C4′−C5′ conformation γ. We also observe a subtle difference in the barrier locations between the Sp *R* and *S* stereoisomers, as indicated in the figures. The structural origins of the barriers are illustrated in Figure 7, which reveals steric crowding in the high-energy regions between χ values of 100° and 150° for the Sp *R* stereoisomer and between χ values of 60° and 110° for the Sp *S* stereoisomer. This energy barrier is due to a close contact between H2′ of the sugar and N3 of Sp for both stereoisomers. When $\chi = 130°$, the distance between H2′ and N3 is 1.90 Å for the *R* stereoisomer but 2.60 Å for the *S* stereoisomer. This makes the *R* stereoisomer crowded and high in energy. However, when $\chi = 80°$, the distance is 2.52 Å for the *R* stereoisomer and 1.89 Å for *S*, so the *S* stereoisomer is crowded and high in energy. Furthermore, the structural reason for the stereoisomer-determined shift in the barriers is shown in Figure S1. The differences in the

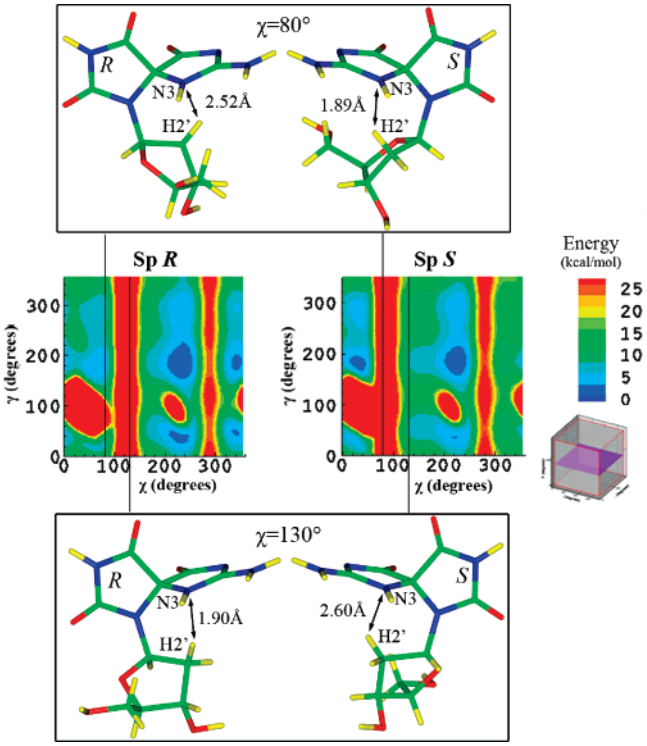

FIGURE 7: Stereoisomeric effects cause energy barrier shifts in *R* and *S* stereoisomers. The sugar conformations are the same in both cases ($P = 160°$ and $\gamma = 180°$).

two stereoisomers cause the O8 atom to have different orientations. The *R* stereoisomer has a close contact between O8 and H2′ in the χ region of 280−300°, while the *S* stereoisomer has a close contact between O8 and H2′ in the χ region of 270−290°.

Statistical Weights. We employed the full set of energy data from the three-dimensional surfaces to compute the fractional statistical weights of each conformer, as described in Methods. Results for variables γ, *P*, and χ are given in Figure 8. The combined statistical weights in C4′−C5′ torsion γ (Figure 8A) show the predominant domains of *gauche*$^+$ (60°) and *trans* (180°) as well as some small statistical weight in the *gauche*$^-$ (300°) region, characteristic of deoxynucleosides and DNA (*70*, *73*). Both the Sp stereoisomers and dG exhibit similar patterns. The statistical weight plot in *P*, the sugar pseudorotation conformation, is given in Figure 8B. The Sp stereoisomers have a distinct preference for the O4′-endo sugar pucker, which differs from the case for unmodified dG (*74*, *75*). This stems from the perpendicular architecture of the Sp stereoisomers, which produces domains of crowding for the usual C2′-endo or C3′-endo DNA sugar conformation which O4′-endo avoids, especially in the *syn* region of χ (Figure S2). In the χ dimension, the Sp *R* stereoisomer favors the *anti* conformation more than *syn* while the *S* stereoisomer favors *syn* over *anti*, but both domains are feasible for each case (Figure 8C). Structurally, this difference can be explained on the nucleoside level, as shown in Figure 9. Specifically, the differences in the *R* and *S* stereoisomers cause the *R* stereoisomer to be more crowded in the *syn* region than the *S*. Note that for the *R* stereoisomer, when the five-membered B-ring of Sp and the sugar are overlaid, the amino group of Sp has much closer contacts with the C5′ and O5′ group of the sugar than the *S* stereoisomer. Unmodified dG on the other hand prefers *syn*

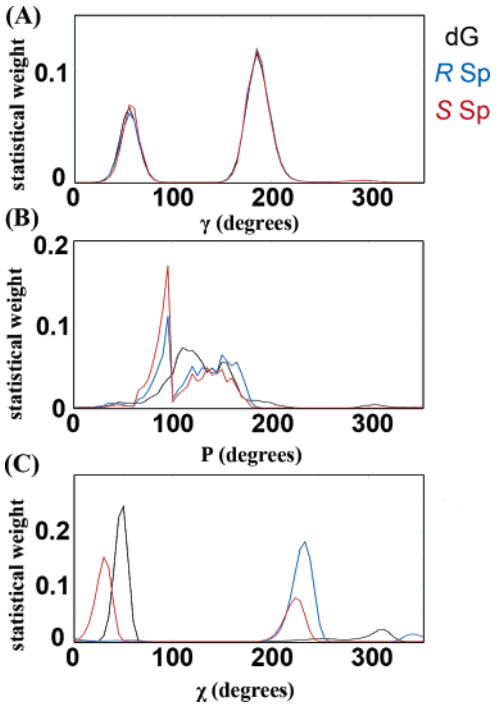

FIGURE 8: Plots of combined statistical weights for variables γ, *P*, and χ.

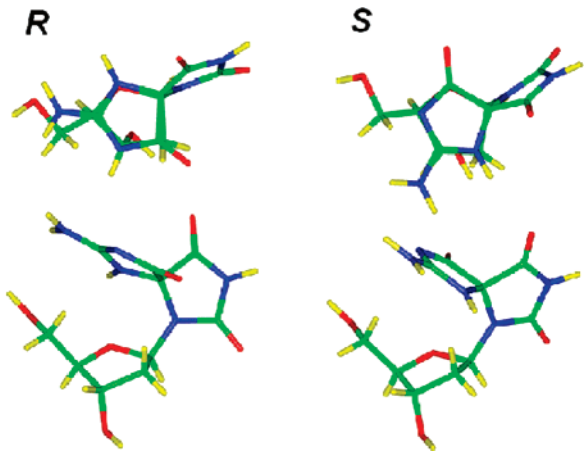

FIGURE 9: Structures of the Sp *R* and *S* stereoisomer deoxyribonucleosides with conformations in which the B-ring of the Sp overlaps the sugar ring, when viewed through the planes of these two rings. The glycosidic torsion angle χ is 35° for the *R* stereoisomer and 70° for *S*. The sugar conformations are the same in both cases ($P = 160°$ and $\gamma = 180°$). The top views are perpendicular to the Sp B-ring, and the bottom views are rotated 90° out of the plane of the paper.

because of a hydrogen bond between the N2−H2 group and O5′ (Figure S3), and hydrogen bonds stabilizing *syn* dG on the nucleoside level are well-known (*57*, *76*).

DISCUSSION

Our structural studies on the base level have delineated the geometries of the Sp *R* and *S* stereoisomers. The QM geometry optimizations reveal a pair of propeller-like, mirror-image structures. Furthermore, the Sp structures are comprised of essentially planar and near-perpendicular five-membered rings, without flexibility at the C4 atom, as determined from the convergence of the nine initial structures to a single one in the case of each stereoisomer. On the

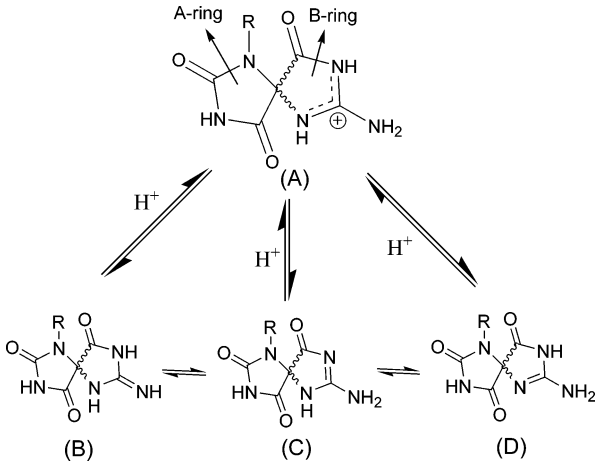

FIGURE 10: Tautomerism and protonation equilibria of Sp.

nucleoside level, our extensive surveys of the potential energy surface reveal restricted rotation about the glycosidic bond compared to unmodified dG. Specifically, an additional barrier between *syn* and *anti* domains is noted. In addition, we find subtle distinctions in the barriers between *syn* and *anti* domains for the *R* and *S* stereoisomers, and the possibility for stereoisomer-dependent *syn* and *anti* preferences is suggested. Lesion-dependent influences on sugar puckering are also found, notably, a preference for O4′-endo puckering for the Sp deoxynucleosides.

Our results are for the amino tautomer (Figure 10C). However, both *R* and *S* stereoisomers of Sp may exist in several tautomeric forms that involve the location of the protons bound to nitrogens in the B-ring (Figure 10). These can be interconverted through a common cation (A). Tautomers that have an exocyclic amino group (C and D) are usually favored over imino tautomers (B) in a variety of heterocyclic ring systems (*77*, *78*). In addition, we have performed QM geometry optimization calculations for the imino tautomer (B) for comparison with the amino tautomer (C) (data not shown). Our results reveal that the amino form (C) is lower in energy by 1 kcal/mol. Of the two tautomers that have an amino group (C and D), we and others (*38*, *46*) prefer C; unlike D, C permits conjugation of the amino group with the carbonyl group in the same ring. However, other tautomers might be possible, and these would merit further investigation if experimental evidence indicating their importance emerged.

The distinct properties of these Sp lesions are expected to have profound influences on DNA structure. If the normal

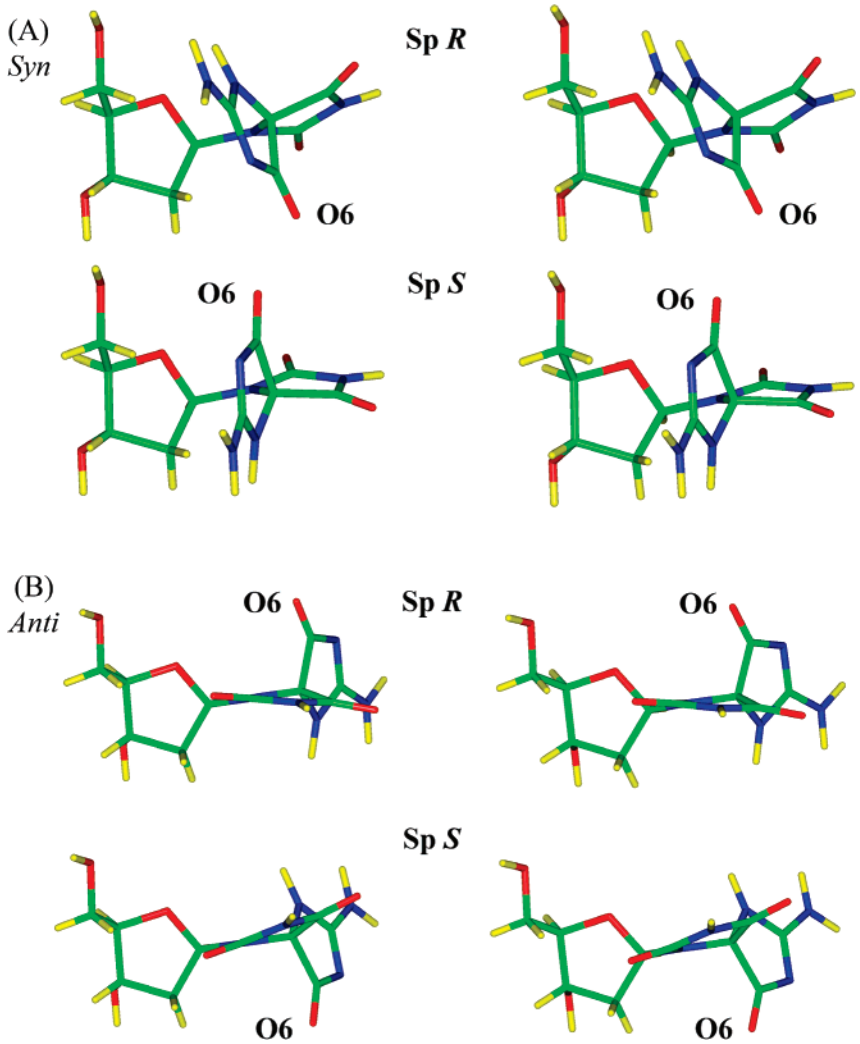

FIGURE 11: Stereoviews of Sp *R* and *S* stereoisomer deoxyribonucleosides in *syn* and *anti* conformations showing the opposite orientation of the O6 atom. The sugar conformations are the same in both cases ($P = 160°$ and $\gamma = 180°$). (A) For the *syn* conformation, χ is 60° for the *R* and 78° for the *S* stereoisomer. (B) For the *anti* conformation, χ is 240° for both *R* and *S* stereoisomers. All stereo images are constructed for viewing with a stereoviewer.

anti glycosidic bond orientation, needed for Watson−Crick base pairing in B-DNA, were adopted, the Sp nucleoside structures suggest that the perpendicular ring system would be inserted into the helix, or cause other very damaging distortions to the double helix; however, *syn* glycosidic conformations would position the Sp structures at the helix exterior (Figure 11). Furthermore, the *syn* conformation would allow for the possibility of base pairing using the N7−H7 group on the remaining Hoogsteen edge opposite adenine or guanine. Molecular modeling studies are currently in progress to investigate the structures of these lesions in DNA duplexes.

The mutagenic consequences of these damaged guanines appear to arise from their unique geometric and steric properties, together with their altered hydrogen bonding capabilities. The steric properties produce diminished flexibility compared to unmodified dG in the glycosidic torsion due to the added rotation barrier, impeding ready *syn*−*anti* interchange. An altered sugar pucker preference is also produced by the lesion. These unique features of the Sp lesions govern their processing within active sites of polymerases and repair enzymes. Furthermore, our results suggest the possibility of differential treatment of the Sp *R* and *S* stereoisomers by replicative or repair enzymes. As shown in Figure 11, the O6 atoms of the stereoisomers are oppositely oriented, offering different hydrogen bonding potentials to enzymes that may treat these lesions. Moreover, the subtle differences in glycosidic bond flexibility manifested in the rotation barriers might be differentially sensed by processing enzymes.

In conclusion, our structural and energetic studies for the Sp stereoisomers show that the structures are mirror images, with near-perpendicular and planar ring systems. The lesions possess unique geometric, steric, and hydrogen bonding features that are stereoisomer-dependent. Treatment of these lesions by replicative and repair enzymes is determined by these unique structural properties.

ACKNOWLEDGMENT

We thank Dr. Brian E. Hingerty for providing the pseudorotation library.

SUPPORTING INFORMATION AVAILABLE

Figure S1 shows stereoisomeric effects causing the energy barrier at ∼285° to be shifted in the *R* and *S* stereoisomers. Figure S2 shows the O5′−N2 and O5′−C2 distances of unmodified dG and Sp *R* and *S* stereoisomers in the *syn* conformation with different sugar puckers. Figure S3 shows a hydrogen bond between O5′ and H2 stabilizing the *syn* glycosidic bond conformation in unmodified dG. Figures S4−S6 show stereoviews of unmodified dG, Sp *R*, and Sp *S* structures with lowest energies in *syn* and *anti* regions. Table S1 shows dihedral angles in starting and final structures for QM geometry optimization of the Sp *R* and *S* stereoisomers. Table S2 shows final coordinates of Sp *R* and *S* stereoisomers after QM geometry optimization. Table S3 shows missing parameters for Sp added to force field. Table S4 shows AMBER atom type and partial charge assignments for the Sp *R* and *S* stereoisomer deoxynucleosides. This material is available free of charge via the Internet at http://pubs.acs.org.

REFERENCES

1. Lindahl, T. (1993) Instability and decay of the primary structure of DNA, *Nature 362*, 709−715.
2. Cadet, J., Berger, M., Douki, T., and Ravanat, J. L. (1997) Oxidative damage to DNA: Formation, measurement, and biological significance, *Rev. Physiol. Biochem. Pharmacol. 131*, 1−87.
3. Henle, E. S., and Linn, S. (1997) Formation, prevention, and repair of DNA damage by iron/hydrogen peroxide, *J. Biol. Chem. 272*, 19095−19098.
4. Fujikawa, K., Kamiya, H., and Kasai, H. (1998) The mutations induced by oxidatively damaged nucleotides, 5-formyl-dUTP and 5-hydroxy-dCTP, in *Escherichia coli*, *Nucleic Acids Res. 26*, 4582−4587.
5. Demple, B., and Harrison, L. (1994) Repair of oxidative damage to DNA: Enzymology and biology, *Annu. Rev. Biochem. 63*, 915−948.
6. Dizdaroglu, M. (1991) Chemical determination of free radical-induced damage to DNA, *Free Radical Biol. Med. 10*, 225−242.
7. Epe, B. (1996) DNA damage profiles induced by oxidizing agents, *Rev. Physiol. Biochem. Pharmacol. 127*, 223−249.
8. Boiteux, S., and Radicella, J. P. (1999) Base excision repair of 8-hydroxyguanine protects DNA from endogenous oxidative stress, *Biochimie 81*, 59−67.
9. Park, Y. J., Choi, E. Y., Choi, J. Y., Park, J. G., You, H. J., and Chung, M. H. (2001) Genetic changes of hOGG1 and the activity of oh8Gua glycosylase in colon cancer, *Eur. J. Cancer 37*, 340−346.
10. Al-Tassan, N., Chmiel, N. H., Maynard, J., Fleming, N., Livingston, A. L., Williams, G. T., Hodges, A. K., Davies, D. R., David, S. S., Sampson, J. R., and Cheadle, J. P. (2002) Inherited variants of MYH associated with somatic G:C→T:A mutations in colorectal tumors, *Nat. Genet. 30*, 227−232.
11. Chevillard, S., Radicella, J. P., Levalois, C., Lebeau, J., Poupon, M. F., Oudard, S., Dutrillaux, B., and Boiteux, S. (1998) Mutations in OGG1, a gene involved in the repair of oxidative DNA damage, are found in human lung and kidney tumours, *Oncogene 16*, 3083−3086.
12. Lu, R., Nash, H. M., and Verdine, G. L. (1997) A mammalian DNA repair enzyme that excises oxidatively damaged guanines maps to a locus frequently lost in lung cancer, *Curr. Biol. 7*, 397−407.
13. Audebert, M., Chevillard, S., Levalois, C., Gyapay, G., Vieillefond, A., Klijanienko, J., Vielh, P., El Naggar, A. K., Oudard, S., Boiteux, S., and Radicella, J. P. (2000) Alterations of the DNA repair gene OGG1 in human clear cell carcinomas of the kidney, *Cancer Res. 60*, 4740−4744.
14. Fan, C. Y., Liu, K. L., Huang, H. Y., Barnes, E. L., Swalsky, P. A., Bakker, A., Woods, J., and Finkelstein, S. D. (2001) Frequent allelic imbalance and loss of protein expression of the DNA repair gene hOGG1 in head and neck squamous cell carcinoma, *Lab. Invest. 81*, 1429−1438.
15. Gu, Y., Desai, T., Gutierrez, P. L., and Lu, A. L. (2001) Alteration of DNA base excision repair enzymes hMYH and hOGG1 in hydrogen peroxide resistant transformed human breast cells, *Med. Sci. Monit. 7*, 861−868.
16. Mori, M., Toyokuni, S., Kondo, S., Kasai, H., Naiki, H., Toichi, E., Hosokawa, M., and Higuchi, K. (2001) Spontaneous loss-of-function mutations of the 8-oxoguanine DNA glycosylase gene in mice and exploration of the possible implication of the gene in senescence, *Free Radical Biol. Med. 30*, 1130−1136.
17. Hamilton, M. L., Van Remmen, H., Drake, J. A., Yang, H., Guo, Z. M., Kewitt, K., Walter, C. A., and Richardson, A. (2001) Does oxidative damage to DNA increase with age? *Proc. Natl. Acad. Sci. U.S.A. 98*, 10469−10474.
18. Osterod, M., Hollenbach, S., Hengstler, J. G., Barnes, D. E., Lindahl, T., and Epe, B. (2001) Age-related and tissue-specific accumulation of oxidative DNA base damage in 7,8-dihydro-8-oxoguanine-DNA glycosylase (Ogg1) deficient mice, *Carcinogenesis 22*, 1459−1463.
19. de Boer, J., Andressoo, J. O., de Wit, J., Huijmans, J., Beems, R. B., van Steeg, H., Weeda, G., van der Horst, G. T., van Leeuwen, W., Themmen, A. P., Meradji, M., and Hoeijmakers, J. H. (2002) Premature aging in mice deficient in DNA repair and transcription, *Science 296*, 1276−1279.

20. Brajter-Toth, A., Goyal, R. N., Wrona, M. Z., Lacava, T., Nguyen, N. T., and Dryhurst, G. (1981) Electrochemical and enzymic oxidation of biological purines, *Bioelectrochem. Bioenerg. 8*, 413−435.
21. Evans, M. D., Dizdaroglu, M., and Cooke, M. S. (2004) Oxidative DNA damage and disease: Induction, repair and significance, *Mutat. Res. 567*, 1−61.
22. Adam, W., Arnold, M. A., Nau, W. M., Pischel, U., and Saha-Moller, C. R. (2002) A comparative photomechanistic study (spin trapping, EPR spectroscopy, transient kinetics, photoproducts) of nucleoside oxidation (dG and 8-oxodG) by triplet-excited acetophenones and by the radicals generated from α-oxy-substituted derivatives through Norrish-type I cleavage, *J. Am. Chem. Soc. 124*, 3893−3904.
23. Misiaszek, R., Crean, C., Joffe, A., Geacintov, N. E., and Shafirovich, V. (2004) Oxidative DNA damage associated with combination of guanine and superoxide radicals and repair mechanisms via radical trapping, *J. Biol. Chem. 279*, 32106−32115.
24. Tretyakova, N. Y., Niles, J. C., Burney, S., Wishnok, J. S., and Tannenbaum, S. R. (1999) Peroxynitrite-induced reactions of synthetic oligonucleotides containing 8-oxoguanine, *Chem. Res. Toxicol. 12*, 459−466.
25. Niles, J. C., Wishnok, J. S., and Tannenbaum, S. R. (2001) A novel nitroimidazole compound formed during the reaction of peroxynitrite with 2′,3′,5′-tri-O-acetyl-guanosine, *J. Am. Chem. Soc. 123*, 12147−12151.
26. Henderson, P. T., Delaney, J. C., Gu, F., Tannenbaum, S. R., and Essigmann, J. M. (2002) Oxidation of 7,8-dihydro-8-oxoguanine affords lesions that are potent sources of replication errors in vivo, *Biochemistry 41*, 914−921.
27. Neeley, W. L., Delaney, J. C., Henderson, P. T., and Essigmann, J. M. (2004) In vivo bypass efficiencies and mutational signatures of the guanine oxidation products 2-aminoimidazolone and 5-guanidino-4-nitroimidazole, *J. Biol. Chem. 279*, 43568−43573.
28. Henderson, P. T., Neeley, W. L., Delaney, J. C., Gu, F., Niles, J. C., Hah, S. S., Tannenbaum, S. R., and Essigmann, J. M. (2005) Urea Lesion Formation in DNA as a Consequence of 7,8-Dihydro-8-oxoguanine Oxidation and Hydrolysis Provides a Potent Source of Point Mutations, *Chem. Res. Toxicol. 18*, 12−18.
29. Niles, J. C., Wishnok, J. S., and Tannenbaum, S. R. (2001) Spiroiminodihydantoin is the major product of the 8-oxo-7,8-dihydroguanosine reaction with peroxynitrite in the presence of thiols and guanosine photooxidation by methylene blue, *Org. Lett. 3*, 963−966.
30. Luo, W., Muller, J. G., and Burrows, C. J. (2001) The pH-dependent role of superoxide in riboflavin-catalyzed photooxidation of 8-oxo-7,8-dihydroguanosine, *Org. Lett. 3*, 2801−2804.
31. Adam, W., Arnold, M. A., Grune, M., Nau, W. M., Pischel, U., and Saha-Moller, C. R. (2002) Spiroiminodihydantoin is a major product in the photooxidation of 2′-deoxyguanosine by the triplet states and oxyl radicals generated from hydroxyacetophenone photolysis and dioxetane thermolysis, *Org. Lett. 4*, 537−540.
32. Sugden, K. D., Campo, C. K., and Martin, B. D. (2001) Direct oxidation of guanine and 7,8-dihydro-8-oxoguanine in DNA by a high-valent chromium complex: A possible mechanism for chromate genotoxicity, *Chem. Res. Toxicol. 14*, 1315−1322.
33. Suzuki, T., Masuda, M., Friesen, M. D., and Ohshima, H. (2001) Formation of spiroiminodihydantoin nucleoside by reaction of 8-oxo-7,8-dihydro-2′-deoxyguanosine with hypochlorous acid or a myeloperoxidase-H_2O_2−Cl^- system, *Chem. Res. Toxicol. 14*, 1163−1169.
34. Suzuki, T., and Ohshima, H. (2002) Nicotine-modulated formation of spiroiminodihydantoin nucleoside via 8-oxo-7,8-dihydro-2′-deoxyguanosine in 2′-deoxyguanosine-hypochlorous acid reaction, *FEBS Lett. 516*, 67−70.
35. Joffe, A., Geacintov, N. E., and Shafirovich, V. (2003) DNA Lesions Derived from the Site Selective Oxidation of Guanine by Carbonate Radical Anions, *Chem. Res. Toxicol. 16*, 1528−1538.
36. Hosford, M. E., Muller, J. G., and Burrows, C. J. (2004) Spermine participates in oxidative damage of guanosine and 8-oxoguanosine leading to deoxyribosylurea formation, *J. Am. Chem. Soc. 126*, 9540−9541.
37. Luo, W., Muller, J. G., Rachlin, E. M., and Burrows, C. J. (2000) Characterization of spiroiminodihydantoin as a product of one-electron oxidation of 8-oxo-7,8-dihydroguanosine, *Org. Lett. 2*, 613−616.
38. Luo, W., Muller, J. G., Rachlin, E. M., and Burrows, C. J. (2001) Characterization of hydantoin products from one-electron oxidation of 8-oxo-7,8-dihydroguanosine in a nucleoside model, *Chem. Res. Toxicol. 14*, 927−938.
39. Martinez, G. R., Medeiros, M. H., Ravanat, J. L., Cadet, J., and Di Mascio, P. (2002) [^{18}O]-labeled singlet oxygen as a tool for mechanistic studies of 8-oxo-7,8-dihydroguanine oxidative damage: Detection of spiroiminodihydantoin, imidazolone and oxazolone derivatives, *Biol. Chem. 383*, 607−617.
40. Vineis, P., Malats, N., Porta, M., and Real, F. X. (1999) Human cancer, carcinogenic exposures and mutation spectra, *Mutat. Res. 436*, 185−194.
41. Fisher, D. E. (2001) The p53 tumor suppressor: Critical regulator of life and death in cancer, *Apoptosis 6*, 7−15.
42. Michaels, M. L., Cruz, C., Grollman, A. P., and Miller, J. H. (1992) Evidence that MutY and MutM combine to prevent mutations by an oxidatively damaged form of guanine in DNA, *Proc. Natl. Acad. Sci. U.S.A. 89*, 7022−7025.
43. Michaels, M. L., Tchou, J., Grollman, A. P., and Miller, J. H. (1992) A repair system for 8-oxo-7,8-dihydrodeoxyguanine, *Biochemistry 31*, 10964−10968.
44. David, S. S., and Williams, S. D. (1998) Chemistry of Glycosylases and Endonucleases Involved in Base-Excision Repair, *Chem. Rev. 98*, 1221−1262.
45. Leipold, M. D., Muller, J. G., Burrows, C. J., and David, S. S. (2000) Removal of hydantoin products of 8-oxoguanine oxidation by the *Escherichia coli* DNA repair enzyme, FPG, *Biochemistry 39*, 14984−14992.
46. Leipold, M. D., Workman, H., Muller, J. G., Burrows, C. J., and David, S. S. (2003) Recognition and removal of oxidized guanines in duplex DNA by the base excision repair enzymes hOGG1, yOGG1, and yOGG2, *Biochemistry 42*, 11373−11381.
47. Hailer, M. K., Slade, P. G., Martin, B. D., Rosenquist, T. A., and Sugden, K. D. (2005) Recognition of the oxidized lesions spiroiminodihydantoin and guanidinohydantoin in DNA by the mammalian base excision repair glycosylases NEIL1 and NEIL2, *DNA Repair 4*, 41−50.
48. Duarte, V., Muller, J. G., and Burrows, C. J. (1999) Insertion of dGMP and dAMP during in vitro DNA synthesis opposite an oxidized form of 7,8-dihydro-8-oxoguanine, *Nucleic Acids Res. 27*, 496−502.
49. Kornyushyna, O., Berges, A. M., Muller, J. G., and Burrows, C. J. (2002) In vitro nucleotide misinsertion opposite the oxidized guanosine lesions spiroiminodihydantoin and guanidinohydantoin and DNA synthesis past the lesions using *Escherichia coli* DNA polymerase I (Klenow fragment), *Biochemistry 41*, 15304−15314.
50. Henderson, P. T., Delaney, J. C., Muller, J. G., Neeley, W. L., Tannenbaum, S. R., Burrows, C. J., and Essigmann, J. M. (2003) The hydantoin lesions formed from oxidation of 7,8-dihydro-8-oxoguanine are potent sources of replication errors in vivo, *Biochemistry 42*, 9257−9262.
51. Halgren, T. A. (1996) Merck molecular force field. I. Basis, form, scope, parametrization, and performance of MMFF94, *J. Comput. Chem. 17*, 490−519.
52. Lee, C., Yang, W., and Parr, R. G. (1988) Development of the Colle-Salvetti correlation-energy formula into a functional of the electron density, *Phys. Rev. B: Condens. Matter Mater. Phys. 37*, 785−789.
53. Becke, A. D. (1988) Density-functional exchange-energy approximation with correct asymptotic behavior, *Phys. Rev. A 38*, 3098−3100.
54. Frisch, M. J., Trucks, G. W., Schlegel, H. B., Scuseria, G. E., Robb, M. A., Cheeseman, J. R., Zakrzewski, V. G., Montgomery, J. A., Jr., Stratmann, R. E., Burant, J. C., Dapprich, S., Millam, J. M., Daniels, A. D., Kudin, K. N., Strain, M. C., Farkas, O., Tomasi, J., Barone, V., Cossi, M., Cammi, R., Mennucci, B., Pomelli, C., Adamo, C., Clifford, S., Ochterski, J., Petersson, G. A., Ayala, P. Y., Cui, Q., Morokuma, K., Malick, D. K., Rabuck, A. D., Raghavachari, K., Foresman, J. B., Cioslowski, J., Ortiz, J. V., Baboul, A. G., Stefanov, B. B., Liu, G., Liashenko, A., Piskorz, P., Komaromi, I., Gomperts, R., Martin, R. L., Fox, D. J., Keith, T., Al-Laham, M. A., Peng, C. Y., Nanayakkara, A., Gonzalez, C., Challacombe, M., Gill, P. M. W., Johnson, B. G., Chen, W., Wong, M. W., Andres, J. L., Head-Gordon, M., Replogle, E. S., and Pople, J. A. (1998) *Gaussian 98*, revision A.7, Gaussian, Inc., Pittsburgh, PA.
55. Berman, H. M., Olson, W. K., Beveridge, D. L., Westbrook, J., Gelbin, A., Demeny, T., Hsieh, S. H., Srinivasan, A. R., and Schneider, B. (1992) The nucleic acid database. A comprehensive

relational database of three-dimensional structures of nucleic acids, *Biophys. J. 63*, 751−759.
56. Altona, C., and Sundaralingam, M. (1972) Conformational analysis of the sugar ring in nucleosides and nucleotides. A new description using the concept of pseudorotation, *J. Am. Chem. Soc. 94*, 8205−8212.
57. Saenger, W. (1984) *Principles of nucleic acid structure*, Springer-Verlag, New York.
58. Hingerty, B. E., Figueroa, S., Hayden, T. L., and Broyde, S. (1989) Prediction of DNA structure from sequence: A build-up technique, *Biopolymers 28*, 1195−1222.
59. Case, D., Pearlman, D., Caldwell, J., Cheatham, T., Ross, W., Simmerling, C., Darden, T., Merz, K., Stanton, R., Cheng, A., Vincent, J., Crowley, M., Ferguson, D., Radner, R., Seibel, G., Singh, U. C., Weiner, P., and Kollman, P. (1997) *AMBER*, version 5.0, University of California, San Francisco.
60. Cornell, W. D., Cieplak, P., Bayly, C. I., Gould, I. R., Merz, K. M., Ferguson, D. M., Spellmeyer, D. C., Fox, T., Caldwell, J. W., and Kollman, P. A. (1995) A Second Generation Force Field for the Simulation of Proteins, Nucleic Acids, and Organic Molecules, *J. Am. Chem. Soc. 117*, 5179−5197.
61. Wang, J. M., Cieplak, P., and Kollman, P. A. (2000) How well does a restrained electrostatic potential (RESP) model perform in calculating conformational energies of organic and biological molecules? *J. Comput. Chem. 21*, 1049−1074.
62. Bayly, C. I., Cieplak, P., Cornell, W., and Kollman, P. A. (1993) A well-behaved electrostatic potential based method using charge restraints for deriving atomic charges: The RESP model, *J. Phys. Chem. 97*, 10269−10280.
63. Hingerty, B. E., Ritchie, R. H., Ferrell, T. L., and Turner, J. E. (1985) Dielectric effects in biopolymers: The theory of ionic saturation revisited, *Biopolymers 24*, 427−439.
64. Xie, X. M., Geacintov, N. E., and Broyde, S. (1999) Stereochemical origin of opposite orientations in DNA adducts derived from enantiomeric anti-benzo[*a*]pyrene diol epoxides with different tumorigenic potentials, *Biochemistry 38*, 2956−2968.
65. Atkins, P. W. (1990) *Physical Chemistry*, 4th ed., W. H. Freeman Co., New York.
66. Mishra, S. K., and Mishra, P. C. (2002) An ab initio theoretical study of electronic structure and properties of 2′-deoxyguanosine in gas phase and aqueous media, *J. Comput. Chem. 23*, 530−540.
67. Hocquet, A., Leulliot, N., and Ghomi, M. (2000) Ground-state properties of nucleic acid constituents studied by density functional calculations. 3. Role of sugar puckering and base orientation on the energetics and geometry of 2′-deoxyribonucleosides and ribonucleosides, *J. Phys. Chem. B 104*, 4560−4568.
68. Haschemeyer, A. E., and Sobell, H. M. (1965) The Crystal Structure of a Hydrogen Bonded Complex of Adenosine and 5-Bromouridine, *Acta Crystallogr. 18*, 525−532.
69. Haschemeyer, A. E., and Sobell, H. M. (1965) The crystal structure of a hydrogen bonded complex of deoxyguanosine and 5-bromodeoxycytidine, *Acta Crystallogr. 19*, 125−130.
70. Gelbin, A., Schneider, B., Clowney, L., Hsieh, S. H., Olson, W. K., and Berman, H. M. (1996) Geometric parameters in nucleic acids: Sugar and phosphate constituents, *J. Am. Chem. Soc. 118*, 519−529.
71. Olson, W. K. (1981) Three-state models of furanose pseudorotation, *Nucleic Acids Res. 9*, 1251−1262.
72. Olson, W. K., and Sussman, J. L. (1982) How Flexible Is the Furanose Ring. 1. A Comparison of Experimental and Theoretical Studies, *J. Am. Chem. Soc. 104*, 270−278.
73. Berman, H. M. (1997) Crystal studies of B-DNA: The answers and the questions, *Biopolymers 44*, 23−44.
74. Olson, W. K. (1982) Computational studies of polynucleotide flexibility, *Nucleic Acids Res. 10*, 777−787.
75. Olson, W. K., and Dasika, R. D. (1976) Spatial Configuration of Ordered Polynucleotide Chains. 3. Polycyclonucleotides, *J. Am. Chem. Soc. 98*, 5371−5380.
76. Olson, W. K. (1973) Syn-anti effects on the spatial configuration of polynucleotide chains, *Biopolymers 12*, 1787−1814.
77. Blackburn, G. M., and Gait, M. J. (1990) *Nucleic acids in chemistry and biology*, Oxford University Press, New York.
78. Elguero, J., Marzin, C., Katritzky, A. R., and Linda, P. (1976) *The tautomerism of heterocycles*, Academic Press, New York.

BI0473657